Mapping and calculation of the shoreline change in selected areas in Tigbauan, Iloilo, Philippines using remote sensing and geographic information systems (GIS) techniques

MAXINNE LOUISE DOMINIQUE L. CO[1], TRISHA MARIE A. LUCIDO[1], GABRIEL DAX P. AGURA[1], ARIS C. LARRODER[1], and PAUL CAESAR M. FLORES[2]

[1]*Philippine Science High School Western Visayas Campus - Department of Science and Technology (DOST-PSHSWVC), Brgy. Bito-on, Jaro, Iloilo City 5000, Philippines*
[2]*The Marine Science Institute, University of the Philippines, Diliman, Quezon City 1101, Philippines*

Article Info	Abstract
	Shoreline change poses a significant threat to coastal environments and is exacerbated by climate change, hence, it should be monitored for better coastal management. This study aimed to determine the shoreline change in Tigbauan, Iloilo using remote sensing and GIS techniques. Eighteen Landsat 5 and 8 images from 1993 to 2020 were obtained using Global Visualization Viewer and processed in Quantum GIS. Shorelines were extracted from processed images and analyzed using the Digital Shoreline Analysis System (DSAS) in ArcGIS by calculating the net shoreline movement, shoreline change envelope, endpoint rate, and linear regression rate. Results showed that from 1993 to 2020, erosion had greater magnitude, rates, and occurrences than accretion. The average rate was -1.022 m per year and erosion was forecasted for most areas in 2030 and 2040. The results can help the government mitigate shoreline erosion risks and methods can be extended to other shorelines.

Introduction. - The rapid changing of shorelines caused by their high vulnerability to natural hazards such as floods, storm impacts, sea-level rise, and coastal erosion, pose a significant threat to coastal environments. With climate change accelerating the occurrence of these natural hazards, shoreline conditions are worsening and better coastal management is needed [1]. Shoreline data is fundamental for coastal management and thus, studies have investigated methods for the accurate detection, mapping, and monitoring of shorelines.

Among the shoreline mapping methods, three main categories have emerged: field testing, aerial photography, and remote sensing [2]. Among the three mapping methods, remote sensing is preferred due to its ability to analyze small changes in the coast as a result of its very long spectral bands and good spatial resolutions. It is also cheaper and can be done through more convenient and accurate methods, such as satellite imagery [3]. To handle satellite data, geographic information system (GIS) programs were utilized with satellite imagery to extract shorelines and calculate parameters through computer-aided tools and methods that reduce manual errors and give researchers full control [4].

Hence, several researchers have studied shoreline change using both remote sensing and GIS techniques. Louati et al. [5] and Sutikno et al. [6] utilized Landsat images and the United States Geological Survey Digital Shoreline Analysis System (USGS DSAS) extension for ArcGIS Copyright© 1995-2015 Esri. [7], Foti et al. [8] used Google Earth Pro and QGIS, while Flores and Siringan [9] utilized Landsat and QGIS. It is notable that among the satellite data used for shoreline studies, the Landsat series images have been proven to offer the best combination of performance and availability due to its open access, large coverage, and long-term data record features [10]. Among the GIS programs for shoreline studies, it was concluded that QGIS is more suitable for editing and georeferencing [11], while the DSAS extension of ArcGIS makes it a better program for shoreline change calculations [7].

Various statistical methods have also been studied and applied to quantify shoreline change, with the most common being the endpoint rate (EPR), average of rates (AOR), and linear regression rate (LRR) [1,12]. However, it is notable that EPR and LRR are more effective [13]. Thus, Landsat images, ArcGIS-DSAS, QGIS, and EPR and LRR were chosen for the analysis of the selected shoreline.

Climate Central [14] identified Tigbauan, Iloilo as one of the many Philippine municipalities that will submerge by 2040. This finding, along with

parameters such as land area, shoreline length, and anthropogenic activities, led to the selection of the Tigbauan Shoreline as the study area. It was verified by the local government unit that there is no data on the Tigbauan shoreline positions and changes. More effective coastal management is necessary for these areas, which requires shoreline data [15,16]. Thus, the study aimed to determine the shoreline change in selected areas in Tigbauan, Iloilo using remote sensing and GIS techniques [10,12].

This study will provide the municipality with important data on shoreline positions, change values, and rates that can help improve their coastal management. Moreover, the methods can also be replicated to determine shoreline change in other areas. Specifically, this research study aimed to:

(i) gather suitable Landsat 4-5 and 8 images from 1993 to 2020 of the selected shoreline using the USGS Global Visualization Viewer (GloVis);

(ii) apply cropping and image enhancement to Landsat images using QGIS 3.10.10 A Coruña;

(iii) trace and extract the shorelines using QGIS;

(iv) calculate the net shoreline movement (NSM) and shoreline change envelope (SCE) using the DSAS extension in ArcGIS 10.4;

(v) calculate the shoreline change rate using the endpoint rate (EPR) and linear regression rate (LRR) methods in DSAS; and

(vi) evaluate the shoreline change over the years.

Methods. - The methods were divided into three main phases: (1) georeferencing of satellite images, (2) digitization of georeferenced images, and (3) shoreline analysis by calculating the shoreline change values and rate statistics.

Study Area. The study area was chosen using four parameters based on previous shoreline change studies: (1) coastal risk projection of Climate Central [14], (2) land area, (3) shoreline length, and (4) locality and infrastructure risk [1,12,16]. The first parameter identified areas that will be submerged by 2040 [14]. The affected land areas were ranked since selecting larger areas would benefit more people. The shoreline lengths were ranked to minimize zoom and increase calculation accuracy. Settlements and infrastructure were also considered. Thus, as seen in Figure 1, the shoreline bordering Barangay 7 and Baguingin in Tigbauan, Iloilo was chosen. It faces the Panay Gulf near the Sibalom River and the observed nearby infrastructures are residential areas and vegetation approximately 15 m from the shoreline.

Figure 1. (a) The study area in the Philippines. (b) The areas in Tigbauan, Iloilo projected to be below the annual flood level in 2040. (c) The shoreline in Tigbauan, Iloilo selected based on the set criteria.

Satellite Image Georeferencing. Landsat 5 and 8 images of the study area from 1993 to 2020 were obtained using GloVis. The images were chosen based on image clarity, cloud coverage, and time and date of image acquisition. The selection process involved scanning all the available images that were taken during the equinox, specifically within the months of August to September. Due to the lack of clear images during these months from 1993 to 1998, images from February and March were used instead. The images with a clear view of the study area, minimal to no cloud cover, and acquisition times ranging from 9:00 AM to 10:30 AM MPST were selected. Those not satisfying the criteria were excluded, resulting in non-uniform intervals. The primary image acquisition date criterion was based on March 20 and September 23 due to the presence of equinoctial tides. A total of 18 Landsat images were used in the study, with five from the March equinox and 13 from the September equinox since during these months, the tidal amplitudes are at a maximum [17]. All images were subjected to visual comparisons and were ensured to have been georeferenced correctly, as determined by the lack of shifts in road alignment.

Image Processing and Shoreline Extraction. The acquired Landsat 4–5 and 8 images underwent image processing using QGIS. The raster images were first uniformly cropped to focus on the identified shoreline. The cropped images were then subjected to geometric and atmospheric corrections using the Semi-automatic Classification Plugin in QGIS [18], DOS1 atmospheric correction, and panchromatic image sharpening. Raster calculation was then performed on the Landsat bands using the Modified Normalized Difference Water Index (MNDWI) with the formula to extract the shoreline positions [19].

$$MNDWI = (Green\ Band - MIR\ Band)/(Green\ Band + MIR\ Band)$$

Where:
Green Band = green band number depending on Landsat type
MIR Band = middle infrared band depending on the Landsat type

Land and water features were further differentiated by utilizing a threshold value of zero in the raster calculator to produce a binary raster image which was then polygonized for shoreline tracing.

Data Analysis. The NSM, SCE, EPR, and LRR were calculated using DSAS in ArcGIS 10.4. Three sets

of shoreline data were calculated and the separation of shoreline images was based on the image acquisition dates. The set 1 and 2 images were acquired near the March and September equinox respectively, while set 3 contained only the earliest and most recent shoreline. The shorelines included in each set are shown in Table 1.

Table 1. Shoreline data used in each calculation.

Set	Shoreline Data (in years)	# of shorelines	Calculations
1	1993, 1996-1998	4	NSM, SCE, EPR, and LRR
2	2004, 2006, 2008, 2009, 2011, 2013-2020	13	NSM, SCE, EPR, and LRR
3	1993, 2020	2	NSM and EPR

The calculation of NSM, SCE, EPR, and LRR values was conducted using the calculate function in DSAS with a 90% confidence interval. ArcGIS-DSAS generated reports for the three sets.

The NSM is the distance between the oldest and earliest shoreline data identified by DSAS based on the exact shoreline dates parameter inputted in ArcGIS. SCE is the greatest distance between each transect. For NSM, positive and negative values mean accretion and erosion respectively, while the SCE is always positive. Both NSM and SCE are in meters. For the EPR, DSAS divided the NSM by the time elapsed between the two shorelines but the variation of the rate over time was not considered. The LRR is the slope of the line generated by a least-squares regression fit to all available shoreline points for each transect. The regression line is the minimum sum of the squared residuals. The squared residual for a data point is the square of the offset distance from the regression line. Both rates are in meters per year.

Results and Discussion. - The results and discussion were divided into six parts namely: acquired satellite images, processed satellite images, traced and extracted shorelines, shoreline change values, shoreline change rates, and shoreline forecasting. All values were generated using the ArcGIS-DSAS function and can be seen in the raw data tables found in the supplementary data section of the journal. Sets 1 and 2 each had a total of 283 transects while set 3 had 294 transects in total.

Acquired Satellite Images. There were 18 Landsat images gathered in total, with nine Landsat 4-5 images from 1993 to 2011, and another nine Landsat 8 images from 2013 to 2020. The images obtained all had spatial resolutions of 30 m, contained clear views of the shoreline, and were captured near the two equinoxes during times ranging from 9:00 AM to 10:30 AM MPST. The tide conditions varied with heights ranging from -0.03 m to 1.67 m. It was determined that three images in set 1, eight images in set 2, and one image in set 3 were taken during low tide. The lack of uniform conditions contributed to increased positional change due to the comparison of shorelines during high and low tides. The images from set 1 and set 2 were also taken in different monsoon seasons, which may affect the tidal conditions. No visible deviations were observed

during the conduct of visual analyses, thus, the georeferenced images were concluded to be correct.

Processed Satellite Images. All satellite images were successfully subjected to image processing techniques starting with uniform cropping, atmospheric correction, and RGB enhancement. The enhanced images increased shoreline definition due to the color contrast in the land and water areas and the use of the water index enhanced the open water features and suppressed the built-up land noise. This enabled the creation of binary raster images with clearly defined separations of the land and water features for easier shoreline extraction.

Traced and Extracted Shorelines. All vector images were cropped and traced based on the study area coordinates. The x-components were the same for all images. However, the y-components of the traced endpoints varied, showing that the shoreline changed over the years. The traced shoreline vectors had sharpened edges due to the 30 m x 30 m pixels, but were not subjected to smoothing to preserve the defined geographical accuracy of the shorelines. Three datasets, shown in Table 1, were then created where images taken near the same equinox were grouped together to ensure uniform conditions for shoreline analysis.

Shoreline Change Analysis. The shoreline change experienced in the study area was analyzed using the SCE and NSM values generated by ArcGIS-DSAS and can be found in the supplementary data section.

Shoreline Change Envelope. The SCE represents the greatest distance among all intersecting shorelines in a given transect. This alone does not indicate if the change is erosional or accretional since it is always positive. The SCE calculations involved set 1 and set 2 shoreline data, shown in Figures 2.a and 2.b, respectively.

The shorelines in set 1 had an average SCE distance of 30.50 m. The greatest distance of 96.24 m in transect 146 showed that the shoreline eroded from 1993 to 1996. For set 1, 55 null values or transects with no observed shoreline position changes were generated, resulting in a minimum distance of 0. These null values were attributed to the low Landsat 4-5 resolution which prevented the detection of changes below 30 m [20].

For set 2, the 13 shorelines were calculated to have an average SCE distance of 61.54 m which is approximately two times greater than that of the previous set or an increase of 101.77%. The greatest distance observed in transect 61 showed that the shoreline accreted by 113.77 m from 2013 to 2020. In set 2, no null values were generated and a minimum distance of 30.01 m was observed in transect 8.

The SCE values show that in the period from March 1993 to 1998, shoreline changes ranged from 0 m to 96.24 m while from September 2004 to 2020, changes ranged from 30.01 m to 113.77 m. These results do not indicate whether the observed changes are mostly erosional or accretional and thus, require

supplemental data from the NSM values. However, it can be said that the greatest changes observed in sets 1 and 2 are erosional and accretional respectively.

Net Shoreline Movement. The NSM represents the distance between the oldest and most recent shorelines for each transect. The NSM values of the 3 sets were generated and analyzed in relation to the SCE values and contained both the negative or erosional and positive or accretional values. The NSM calculations involved all three sets of shoreline data, shown in Figures 3.a for set 1, 3.b for set 2, and 3.c for set 3.

For set 1, among the 283 transects, 47% or 133 were erosional, 25.09% or 71 were accretional, while 27.9% or 79 were null. The maximum negative value of -64.16 m at transect 146 also had the greatest SCE of 96.24 m from 1993 to 1996. This suggests that from 1996 to 1998, transect 146 accreted by 32.08 m. The shoreline changes from March 1993 to 1998 ranged from -64.16 m to 63.17 m. The average distances indicate that despite having greater accretion in terms of magnitude, the presence of more erosional transects led to an average distance of -6.04 m, which is considered erosional.
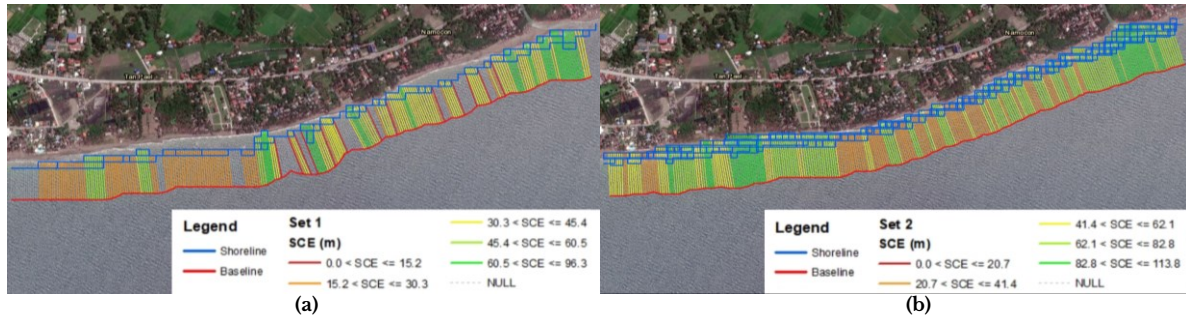

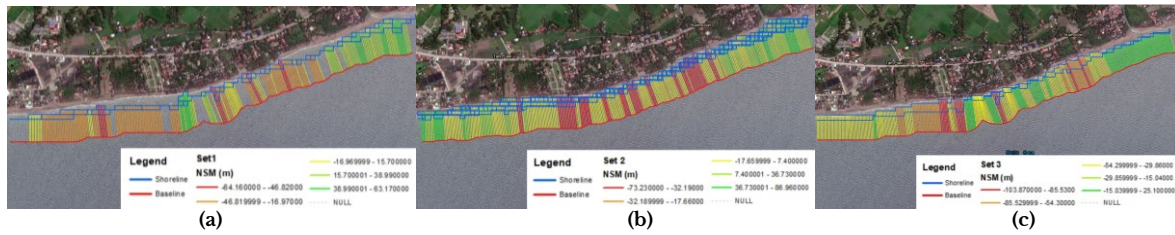**Figure 2.** The shoreline change envelopes of (a) set 1, and (b) set 2.

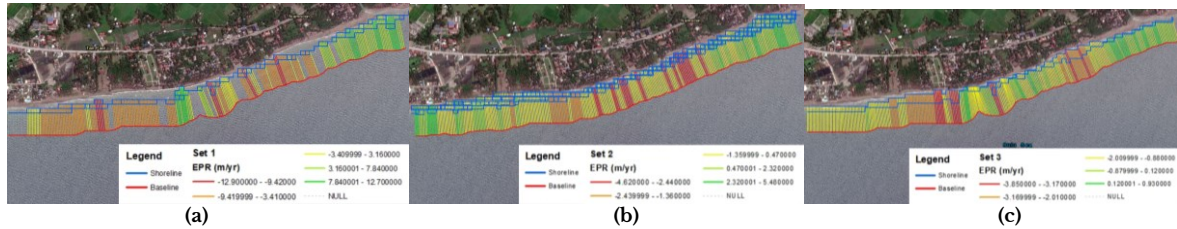**Figure 3.** The net shoreline movements of (a) set 1, (b) set 2, and (c) set 3.

Figure 4. The endpoint rates of (a) set 1, (b) set 2, and (c) set 3.
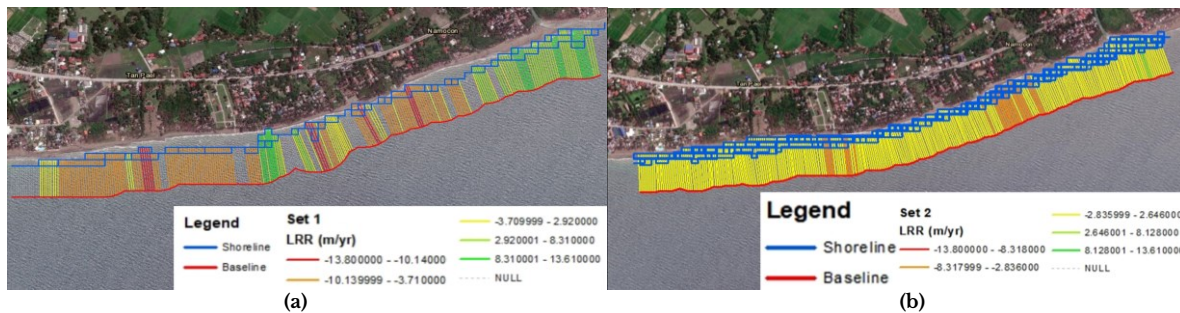

Figure 5. The linear regression rates of (a) set 1, and (b) set 2.

Relative to set 1, the average erosion in set 2 decreased by 13.58 m while the average accretion decreased by only 3.22 m. The positive distances were also greater than the negative distances. These show that from 2004 to 2020, more parts of the shoreline eroded but the accretional areas had greater changes resulting in an average of only -1.99 m, which is 67.05% less than that of set 1.

Set 3 had the most and least number of erosional and accretional transects with 90.82% and 9.18% of the total, respectively. The shoreline changes ranged from -103.37 m to 25.1 m. The high maximum erosion and number of erosional transects contributed to a high average erosion of -41.3 m, while the average accretion was only 19.25 m. Thus, the average NSM from 1993 to 2020 was -35.74 m.

The average NSM in set 3 is significantly greater than that of sets 1 and 2. This high average can be attributed to the high shoreline erosion from 1998 to 2004 since the changes during this period were not investigated due to image availability.

Shoreline Change Rate Analysis. The rate of change experienced by the shoreline was calculated using the EPR and LRR methods in ArcGIS-DSAS and can be found in the supplementary data section.

Endpoint Rate. The EPR calculates the shoreline change rate based on only two shorelines. The average NSM distances were divided by the time elapsed between the oldest and most recent shorelines to generate the EPR values. The EPR calculations involved all three sets of shoreline data, shown in Figures 4.a for set 1, 4.b for set 2, and 4.c for set 3.

For set 1, the null transects prevented DSAS from determining the average CI associated with rates, reduced n, uncertainty, and transects with statistically significant erosion or accretion. The maximum rates for set 1 are significantly greater than that of the other sets while the average rates lowered to values closer to that of the other sets, leading to an EPR of -1.21 m per year.

For set 2, 35.94% of the 192 erosional transects and 96.70% of the 91 accretional transects were statistically significant. Accretional rates were also greater than the erosional rates. These explain why despite having more erosional transects, the average NSM and EPR of this set are low, leading to set 2 having the least EPR of -0.13±0.89 m per year.

Set 3 had the lowest maximum erosion rate and an average erosion rate that is only 50.83% of set 1. However, it had the lowest accretion rates, leading to set 3 having the highest average EPR of -1.32±0.52 m per year.

Linear Regression Rate. The LRR used all available shorelines to determine the change rate and was performed for sets 1 and 2, shown in Figures 5.a and 5.b, respectively.

The LRR of set 1 had fewer null transects than the EPR, showing that more changes occurred in 1996 and 1997. The maximum rates increased by less than 1 m per year with the addition of the 1996 and 1997 shorelines, but the average rates significantly increased by more than 100% of the EPR rates. This showed that the shoreline experienced more changes in 1996 and 1997 compared to just 1993 and 1998. However, the LRR of -1.23 m per year differed from the EPR by only 0.02 m, suggesting that despite having more changes, the erosion and accretion rates still balanced out to result in a similar average rate.

The LRR of set 2, shown in Figure 5 (b), had more erosional and less accretional transects than the EPR. This was also true for transects with statistically significant erosion and accretion. These can be attributed to the shorelines that were not included in the EPR calculations. The average erosion and accretion rates were greater and lesser, respectively, than the EPR. The LRR of -1.22±0.72 m per year is nine times the EPR which also indicates that despite the few differences in the 2004 and 2020 shorelines, the shorelines between them experienced more erosion and less accretion, resulting in the high erosional LRR.

Shoreline Forecasting. Using the LRR of set 2, the DSAS forecaster predicted that in 2030 and 2040, erosion will occur in most transects while accretion is observed in areas near the shoreline ends but are mixed with erosional transects. The part of the shoreline from 10° 40' 7.413" to 10° 40' 19.7292"N latitude and 122° 23' 27.4266" to 122° 24' 12.4158"E longitude is expected to erode by 2030 and 2040 and these areas contain most of the human settlements in the study area.

Figure 6. The forecasted shoreline positions for 2030 and 2040.

Limitations. The study utilized shorelines from years with Landsat images that fit the set criteria, thus, not all years from 1993 to 2020 were included in the calculations. Due to availability, low-resolution images were utilized resulting in the presence of null transects which prevented the calculation of certain values. No physical investigations were conducted due to safety concerns amidst the pandemic. Further investigation of the factors affecting the identified shoreline changes, as well as the verification of the predicted shoreline positions, was not performed.

Conclusion. - The shoreline change values showed that more parts of the shoreline eroded from 2004 to 2020 but a greater magnitude of erosion was observed from 1993 to 1998. The erosion from 1993 to 2020 was significantly greater than that of the other sets, suggesting that most occurred from 1998 to 2004. This was supported by the EPR and LRR calculations which showed that the 1993 and 2020 shorelines also had the least accretion rates and the most and least transects with statistically significant erosion and accretion respectively. It can be concluded that the

shoreline in Tigbauan, Iloilo experienced more erosion than accretion in both occurrence and magnitude from 1993 to 2020. The average shoreline change rates ranged from -0.13 to -1.32 m per year, showing that the shoreline is eroding at an average change rate of -1.022 m per year. The average LRR from September 2004 to 2020 was used to forecast that erosion will continue in 2030 and 2040 for the majority of the shoreline. These data can be used to improve the municipality's coastal management by identifying which areas are vulnerable to shoreline erosion and coastal area loss.

Recommendations. - More shoreline images with better resolutions are recommended to provide more accurate shoreline change rates. An effective smoothing function with a clearly defined accuracy may also be applied to extracted shoreline vectors prior to shoreline calculation. Moreover, adding the tidal level and monsoon season to the image criteria and considering the digitization uncertainty will enable more uniform shoreline conditions and accurate calculations. Physical shoreline inspection should be conducted to obtain more information that could contribute to the analysis. Supplementary data such as daily rainfall, typhoon tracks, and conducted human activities are recommended to understand the factors affecting shoreline change. Lastly, the shoreline change rate should be verified further so it can be utilized to accurately predict future shoreline positions.

References

[1] Armenio E, Serio FD, Mossa M, Petrillo AF. 2019. Coastline evolution based on statistical analysis and modeling. Natural Hazards and Earth System Sciences. 19(9): 1937–1953.

[2] Aryastana P, Ardantha IM, Candrayana KW. 2018. Coastline change analysis and erosion prediction using satellite images. MATEC web of conferences. 197: 13003.

[3] Parthasarathy KSS, Deka PC. 2019. Remote sensing and GIS application in assessment of coastal vulnerability and shoreline changes: a review. ISH Journal of Hydraulic Engineering. 1–13.

[4] Kostecki R. 2018. Application of the spatial database for shoreline change analysis and visualisation: Example from the western polish coast, southern Baltic sea. Quaestiones Geographicae. 37(3): 25–34.

[5] Louati M, Saïdi H, Zargouni F. 2014. Shoreline change assessment using remote sensing and GIS techniques: a case study of the Medjerda delta coast, Tunisia. Arabian Journal of Geosciences. 8(6): 4239–4255.

[6] Sutikno S, Sandhyavitri A, Haidar M, Yamamoto K. 2017. Shoreline change analysis of peat soil beach in bengkalis island based on GIS and RS. IACSIT International Journal of Engineering and Technology. 9(3): 233–238.

[7] Thieler E, Himmelstoss E, Zichichi J, Ergul A. 2017. Digital Shoreline Analysis System (DSAS) version 4.0—An ArcGIS extension for calculating shoreline change. U.S. Geological Survey Open-File Report. 2008–1278.

[8] Foti G, Barbaro G, Bombino G, Fiamma V, Puntorieri P, Minniti F, Pezzimenti C. 2019. Shoreline changes near river mouth: case study of Sant'Agata River (Reggio Calabria, Italy). European Journal of Remote Sensing. 52(4): 102–112.

[9] Flores PC, Siringan F. 2020. Shoreline Change in Response to the Construction of a Flood Canal in Jaro, Iloilo City, Philippines. IEEE India Geoscience and Remote Sensing Symposium (InGARSS). 134-137.

[10] Liu Y, Wang X, Ling F, Xu S, Wang C. 2017. Analysis of coastline extraction from Landsat-8 OLI imagery. Water. 9(11): 816.

[11] Friedrich C. 2014. Comparison of ArcGIS and QGIS for Applications in Sustainable Spatial Planning [thesis]. [Masterarbeit]: University of Vienna.

[12] Deepika B, Avinash K, Jayappa KS. 2013. Shoreline change rate estimation and its forecast: remote sensing, geographical information system and statistics-based approach. International Journal of Environmental Science and Technology. 11(2): 395–416. doi:10.1007/s13762-013-0196-1.

[13] Foster ER, Savage RJ. 1989. Methods of Historical Shoreline Analysis, in: Proc. Coastal Zone '89, ASCE, New York, USA.

[14] Climate Central Organization. Coastal Risk Screening Tool: Sea level rise and coastal flood risk maps. Climate Central. [accessed 2020 December 12]. Available from: https://coastal.climatecentral.org/map.

[15] Department of Environment and Natural Resources, Bureau of Fisheries and Aquatic Resources of the Department of Agriculture, and Department of Interior and Local Government. 2001. Philippine Coastal Management Guidebook No. 8: Coastal Law Enforcement. Coastal Resource Management Project of the Department of Environment and Natural Resources, Cebu City, Philippines, 164 p.

[16] Bañas JCC, Subade RF, Salaum DN, Posa CT. 2019. Valuing vanishing coasts: The case of Miagao coastline in Southern Iloilo, Philippines. Ocean & Coastal Management.

[17] Sridharan S. 2017. Solar and lunar tidal variabilities in GPS-TEC and geomagnetic field variations: Seasonal as well as during the sudden stratospheric warming of 2010. Journal of Geophysical Research: Space Physics. 122(4): 4571–4587.

[18] Congedo L. 2020. Semi-Automatic Classification Plugin Documentation Release 7.0.0.1.

[19] Xu H. 2006. Modification of Normalized Difference Water Index (NDWI) to Enhance Open Water Features in Remotely Sensed Imagery. International Journal of Remote Sensing. 27. 3025–3033.

[20] White K, Asmar HME. 1999. Monitoring changing position of coastlines using Thematic Mapper imagery, an example from the Nile Delta. Geomorphology. 29(1-2): 93–105. doi: 10.1016/s0169-555x(99)00008-2.